Title: Analysis of auto-ignition of heated hydrogen–air mixtures with different detailed reaction mechanisms

Authors: I. Stanković, B. Merci

In: Combustion Theory and Modelling, Volume 15, Issue 3, Pages 409-436.

I. Stanković, B. Merci. (2011) Analysis of auto-ignition of heated hydrogen–air mixtures with different detailed reaction mechanisms. *Combustio, Theory and Modelling*. 15:409-436,2011 (DOI: 10.1080/13647830.2010.542830)

Vol. , No. , , 1–26

Analysis of auto-ignition of heated hydrogen/air mixtures with different detailed reaction mechanisms

I. Stanković[a*] and B. Merci[a]

[a]*Department of Flow, Heat and Combustion Mechanics, Ghent University - UGent, 41 St.-Pietersnieuwstr., 9000 Gent Belgium*

(*Received 00 Month 200x; final version received 00 Month 200x*)

Auto-ignition processes of hydrogen, diluted with nitrogen, in heated air are numerically investigated by means of an unsteady laminar flamelet approach in mixture fraction space. The focus is on the auto-ignition delay time and the most reactive mixture fraction as obtained with five chemical mechanisms. Two strongly different levels of dilution, corresponding to experiments in the open literature, are considered. This concerns low-temperature chemistry at atmospheric pressure. The temperature of the air stream is much higher than the temperature of fuel stream in the cases under study. We extensively investigate the effect of the co-flow temperature, the conditional scalar dissipation rate and the resolution in mixture fraction space for one case. With respect to the conditional scalar dissipation rate, we discuss the Amplitude Mapping Closure (AMC) model with imposed maximum scalar dissipation rate at mixture fraction equal 0.5, as well as a constant conditional scalar dissipation rate value over the entire mixture fraction value range. We also illustrate that an auto-ignition criterion, based on a temperature rise, leads to similar results as an auto-ignition criterion, based on OH mass fraction, provided that the hydrogen is not too strongly diluted.

Keywords: Combustion; Auto-ignition; Kinetics; Hydrogen; Hot air co-flow

*Corresponding author. Email: Ivana.Stankovic@UGent.be; Tel.: +32 9 264 33 00; Fax: +32 9 264 35 75

ISSN: print/ISSN online

DOI:
http://www.informaworld.com

Nomenclature

c_{p_η}	conditional specific heat capacity at the constant pressure
erf	error function
h	enthalpy
n	number of species
N	scalar dissipation rate
Q	conditionally averaged reactive scalar
R	reaction
t	time
T	temperature
W	chemical reaction rate
Y	species mass fraction

Greek letters

η	sample space variable for the mixture fraction
τ	delay time
ξ	mixture fraction

Subscripts

cf	co-flow
$fuel$	fuel
i	species index
ign	ignition
max	related to the largest value
mr	most reactive
p	pressure
st	stoichiometric
η	conditioned on $\xi = \eta$

Other special symbols

$\langle \cdot \mid \eta \rangle$	conditioning

1. Introduction

Auto-ignition plays an important role in many practical combustion devices. Obvious examples are modern low NO_x homogeneous charge compression injection (HCCI) engines and lean premixed pre-vaporised gas turbines. Also in lifted flames, auto-ignition related chemistry strongly affects the flame lift-off height (e.g. [1]). Typically, this concerns chemistry at relatively low temperature, in the order of 1000K and less. It is instructive to investigate to what extent existing H_2/O_2 chemistry mechanisms are applicable at these low temperatures. This is the first motivation for the study of the present paper, which fits in our research on the combined application of LES (Large-Eddy Simulations) and CMC (Conditional Moment Closure) [2] to simulate auto-ignition [3] and lifted flames. Two well-documented experiments will be pursued: the study of Markides [4] and the Cabra flame [5]. In both experiments, the fuel is hydrogen, diluted with nitrogen, igniting after mixing with hot air co-flow. The levels of dilution are strongly different. In the study of [4], different regimes were encountered, depending on the fuel and air mass flow rates and temperatures, ranging from attached flames over lifted flames to a "random spots regime". The Cabra flame is a lifted flame.

In a number of RANS (Reynolds-Averaged Navier-Stokes) CFD simulations [1, 5–10] and a few Large-Eddy Simulations (LES) [3, 11, 12] results for hydrogen flames [4, 5] are presented. Common to all these studies is the revelation that detailed chemical kinetics need to be used to accurately describe the mechanisms that determine flame stabilization. In [3] we show that for the Markides case [4], the flame is stabilized by auto-ignition in our simulations what is in agreement with the statements in [4]. While a RANS-CMC study [9] of the Cabra case [5] states that auto-ignition stabilization is possible only for higher temperatures, the strong dependence of the lift-off hight on the co-flow temperature shows that chemistry is still important. In [1] it is also concluded that "the flame is largely controlled by the chemical kinetics".

As chemistry plays an important role in the determination of the location of the random spots or the flame lift-off height in the numerical simulations, we focus on chemistry solely in the present paper. Thus, we do not consider transport effects (convection and diffusion) in physical space, so that effectively we apply an Unsteady Laminar Flamelet model [13, 14]. This is in line with the recommendation of [15]: "the reader is encouraged to always perform laminar transient simulations, in either physical or mixture fraction space, for any turbulent non-premixed auto-ignition problem considered".

In the context of [5], some chemistry studies have already been reported. In [1], results obtained with the mechanism of [16] are compared to what is obtained with a "stripped" version of the GRI2.1 [17] mechanism. Reaction rates of certain reactions are also modified to illustrate their effect. In [10], the mechanisms of [16] and [18] are compared, again in terms of the effect on the flame lift-off height. It is stated that the Cabra flame [5] is dominated by chemistry. These statements further motivate the present work. Moreover, while the conclusions of [1], [6] and [10] are very important, the chemistry study in those references was limited to the effect on the lift-off height of only a few chemistry mechanisms. This can be translated into the effect on auto-ignition delay.

In the present work, we report results of a more extensive study of different chemistry mechanisms. To be more precise, we consider five different schemes, including two of the schemes used in [1, 6, 10]:

- Li et al. [18];
- O'Conaire et al. [19];
- Mueller et al. [16];
- Yetter et al. [20] and
- Konnov [21].

Moreover, we do not only consider the auto-ignition delay time, but also the "most reactive mixture fraction" [15]. Two criteria for auto-ignition are compared. The first criterion is based on the OH species mass fraction [10], while the second relies on a temperature rise [11]. We investigate the influence of the co-flow air temperature and of the conditional scalar dissipation rate. For the case of [4], we also discuss the effect of the resolution in mixture fraction space. Finally, we discuss similarities and differences in the results, depending on the level of dilution of hydrogen by nitrogen. To the best of the authors' knowledge, no such extensive chemistry study, for the cases under study, has been reported yet.

2. Numerical Set-Up

2.1 Test Cases

Table 1 summarizes the fuel and co-flow composition and temperature range considered, in line with the values for the experiments of [4] and [5], respectively. The composition and temperatures are the boundary conditions for the calculations. The initial conditions are defined as inert mixing of fuel and oxidizer. Figure 1 shows the initial profiles for both cases. A zoom in the region $0 < \eta < 0.1$ is also shown in Fig. 1, as this will be the region where auto-ignition takes place (see below). The two most obvious differences between the two cases are the level of hydrogen dilution and the fuel temperature, causing a substantially different fuel mass density (Figure 2). The dilution will strongly affect the results, while the fuel temperature is effect of secondary order, as discussed below.

Due to the difference in fuel composition, the stoichiometric mixture fraction is also strongly different. It is much higher for the Cabra flame (0.474) than for the Markides case (0.184).

2.2 Chemistry Mechanisms

H_2/O_2 chemistry kinetics can be described with a number of different detailed comprehensive chemical mechanisms, which have been tested and validated for experimental data over a range of physical conditions. Some mechanisms have been optimized for the combustion of pure hydrogen, but most of them are sub-mechanisms of hydrocarbon combustion schemes. In this study, five chemical mechanisms for hydrogen combustion are tested. Reaction mechanisms for H_2-O_2 combustion, developed by different authors, basically differ by the number of reactions and their rate constants.

Yetter et al. [20] presented a detailed mechanism containing 19 reversible reactions and 9 species (H_2, H, O, O_2, OH, H_2O, HO_2, H_2O_2, and N_2). The mechanism is summarized in Table 2. The hydrogen/oxygen system is in fact a sub-mechanism of the mechanism for a carbon monoxide/hydrogen/oxygen system [20]. The mechanism was validated, using experimental data obtained from shock tube experiments and various types of reactor experiments within a temperature range (823K - 2870K), with equivalence ratios between 0.0005 and 6.0 and pressure between 0.3atm and 2.2atm. The uncertainties in the model are estimated as $\pm$10%, except for HO_2 [20].

Mueller et al. [16] adjusted this mechanism to match experimental data for a wider pressure range (0.3atm - 15.7atm) and more narrow low temperature range (850K - 1040K). The resulting scheme [16] involves the same 19 reactions (Table 2). The mechanism was extensively studied at flow reactor conditions, but it was not tested for other types of experiments.

Subsequently, Li et al. [18] updated this H_2/O_2 mechanism, based upon more recent thermodynamic data and rate coefficients validated against a wider range of experimental conditions (298K - 3000K, 0.3atm - 87atm). The mechanism was compared to the follow-

ing experimental data: laminar flame speed, shock tube ignition delay time, and species profiles in various pressure flow reactors (VPFR), shock tube, and burner-stabilized flame studies. The model predictions agreed well with experimental data for all VPFR cases (which were also used for the validation of the Mueller et al. [16] mechanism). The good agreement with the experimental data demonstrates that the mechanism has excellent predictive capabilities for different experimental systems. The following parameters were revised:

- the formation enthalpy of OH;
- the rate constant of the branching reaction: H + O_2 = O + OH (R1);
- the rate constant of: H + OH + M = H_2O + M (R8);
- the low-pressure-limit rate constant of the competitive reaction: H + O_2 (+ M) = HO_2 (+ M) (R9).

O'Conaire et al. [19] also developed a comprehensive H_2/O_2 chemistry mechanism, starting from [16], again consisting of the same 19 reactions of Table 2. It was validated for a wide temperature range (298K - 2700K), pressure range (0.05atm - 87atm) and equivalence ratio range (0.2 - 6). They reported that in the shock tubes, predictions of ignition delay time at atmospheric pressure are in good agreement with experimental data. The model was also successfully validated with experimental data from flow reactors and laminar premixed flames. At all flow reactor conditions the mechanism exhibits almost identical behaviour to the original scheme of [16]. The differences between the Li mechanism and the O'Conaire mechanism are in the reaction rate constants of the reactions R1, R8, R9 and R17.

More recently, Konnov [21] presented a different mechanism, not starting from [16]. The validation range covers ignition experiments from 950K to 2700K and pressures up to 87atm; hydrogen oxidation in a flow reactor at temperatures around 900K from 0.3atm up to 15.7atm; flame burning velocities in hydrogen-oxygen-inert mixtures from 0.35atm to 4atm; and hydrogen flame structure at 1atm and 10atm. The mechanism consists of 21 reversible reactions, with the same 9 species as for the other schemes. The mechanism showed good quantitative agreement with the observed ignition experiments, and with the measurements in the flow reactor at 0.3atm, 1atm and 6.5atm. At higher pressure, the hydrogen concentrations agree well with the experimental results in the lean mixtures. The rate of hydrogen oxidation in the stoichiometric mixtures was significantly underpredicted. Konnov included the reaction: H + HO_2 = H_2O + O while the other authors did not include it in their mechanisms, arguing that it is kinetically similar to reaction R11 of Table 2. Konnov also included the following reaction for completeness: H_2 + O_2 = OH + OH. The reverse reaction, -R10, leads to chain initiation in hydrogen-oxidation mixtures together with this reaction. Michael et al. [22] measured the total rate of initiation, and concluded that the net effect of this reaction is negligible.

The H_2/O_2 chain reactions, R1-R4, play a prominent role for the composition of the radical pool. In [1] it was shown that reactions R1-R3 are reactions to which auto-ignition is most sensitive. The reactions R5-R8 describe the dissociation/recombination of H_2/O_2 while R9-R19 describe the formation and consumption of the HO_2 and H_2O_2.

In the present paper, we focus on the behaviour of the different mechanisms in terms of low-temperature auto-ignition in non-homogeneous mixtures, which resembles the situation in physical space in the experiments of [4] and [5]. We also perform a sensitivity study to explain some differences observed in the results (Section 3.3).

2.3 Modelling

We use the stand-alone code 0D-CMC [23] to perform the calculations. This code was developed, starting from the more general CMC method [2], in which (at least) trans-

port equations are solved for conditionally averaged reacting scalars, Q_i, conditioned on mixture fraction:

$$Q_i \equiv \langle Y_i \mid \xi = \eta \rangle \equiv \langle Y_i \mid \eta \rangle, i = 1, ..., n \tag{1}$$

where η is the sample space variable for the conserved scalar ξ (mixture fraction) and the operator $\langle \cdot \mid \xi = \eta \rangle$, briefly $\langle \cdot \mid \eta \rangle$, denotes ensemble averaging subject to the fulfillment of the condition on the right hand side of the vertical bar. The equations are solved for all n species of the reaction mechanism. In addition hereto, a transport equation for conditional mean temperature is solved. Not accounting for any transport in physical space, the CMC equations boil down the "unsteady laminar flamelet model" equations (e.g. [13, 14]). The following equations are solved:

$$\frac{\partial Q_i}{\partial t} = \langle N \mid \eta \rangle \frac{\partial^2 Q_i}{\partial \eta^2} + \langle W_i \mid \eta \rangle \tag{2}$$

$$\frac{\partial Q_T}{\partial t} = \langle N|\eta \rangle \left[\frac{1}{c_{p_\eta}} \left(\frac{\partial c_{p_\eta}}{\partial \eta} + \sum_{i=1}^{n} c_{p,i_\eta} \frac{\partial Q_i}{\partial \eta} \right) \frac{\partial Q_T}{\partial \eta} + \frac{\partial^2 Q_T}{\partial \eta^2} \right] - \frac{1}{c_{p_\eta}} \left\langle \sum_{i=1}^{n} h_i W_i \middle| \eta \right\rangle \tag{3}$$

where $c_{p_\eta} \equiv \left\langle c_p \mid \eta \right\rangle$ is the conditional specific heat capacity at constant pressure.

The conditional reaction rates are calculated, based on the conditional mean values of the arguments (as in first order CMC):

$$\langle W_i \mid \eta \rangle = W_i(Q_i, Q_T) \tag{4}$$

The chemical reaction rates W_i are obtained from the detailed chemical mechanisms and evaluated using the CHEMKIN package [24].

The conditional scalar dissipation rate, $\langle N \mid \eta \rangle$, determines the level of molecular mixing. It can be modelled with the Amplitude Mapping Closure model (AMC) [25]. The AMC model represents the conditional scalar dissipation rate in a counterflow configuration. It is considered to have a bell shape (function $G(\eta)$):

$$\langle N \mid \eta \rangle = N_0 G(\eta) \tag{5}$$

where

$$G(\eta) = exp(-2(erf^{-1}(2\eta - 1))^2) \tag{6}$$

and

$$N_0 = \frac{N}{\int_0^1 G(\eta) P(\eta) d\eta} \tag{7}$$

where N is the unconditional scalar dissipation rate. The model is implemented here as:

$$\langle N \mid \eta \rangle = exp(-2(erf^{-1}(2\eta - 1))^2) N_{max} \tag{8}$$

where erf^{-1} is the inverse error function. The AMC model is parametrized by its maximum value ($N_0 = N_{max}$), imposed at η = 0.5. Fig. 3 shows the profile corresponding to this expression. Below, we also discuss results when N_{max} is imposed over the entire mixture fraction range (also shown in Fig. 3), as well as the sensitivity of the results to N_{max}.

For the solution of Equations (2) and (3), the mixture fraction range [0:1] is discretized into a number of bins, i.e. a computational mesh in mixture fraction space. In our basic set-up, the number of bins in mixture fraction space is 51, clustered around the "most reactive mixture fraction". The ODE system is integrated by the package VODPK [26].

2.4 Auto-ignition criterion

In the literature, several criteria are used to determine the moment of the ignition. In [11], auto-ignition is defined as the moment when the maximum local temperature is 1% higher than the nominal co-flow temperature for a certain mixture fraction value. In [10], auto-ignition is defined as the moment when the maximum mass fraction of OH reaches 2×10^{-4} for a certain mixture fraction value. We compare these two criteria below. Regardless of the criterion, the "most reactive mixture fraction", η_{mr}, is the mixture fraction for which the auto-ignition occurs first [15].

3. Results and discussion

Unless mentioned otherwise, the criterion of [10] is applied to determine "auto-ignition" and results are presented for constant conditional scalar dissipation rate over the entire mixture fraction range and with 51 bins in mixture fraction space, clustered around η_{mr}.

3.1 Test case of Markides [4]

3.1.1 Observations during the auto-ignition process

We first illustrate the temporal evolution of OH mass fraction during the auto-ignition, as it plays an important role in the auto-ignition process. Fig. 4 shows results for the studied chemical mechanisms during the initial stages of auto-ignition for the fuel temperature (T_{fuel}) equal to 691K, co-flow temperature (T_{cf}) equal to 1030K and constant scalar dissipation rate $\langle N \mid \eta \rangle = 1\text{s}^{-1}$. The results are presented for times, for each mechanism normalized by their own auto-ignition delay time (Table 3). After the onset of auto-ignition, there is a fast and substantial increase in maximum OH mass fraction. The peak value moves towards the stoichiometric mixture fraction ($\eta_{st} = 0.184$). The most reactive mixture fraction (Table 3), η_{mr}, is on the lean side. Differences between the mechanisms are small, except for the Konnov mechanism [21], where the evolution towards η_{st} is slower in terms of t/τ_{ign}. However, $t = 2 \times \tau_{ign}$ for this scheme corresponds to $t = 1.5 \times \tau_{ign}$ for the Yetter mechanism [20], so that in "in absolute time" the Konnov mechanism [21] is in fact faster. Note that the "end" result, for $t = 10 \times \tau_{ign}$, is identical for all schemes, as identical thermal property file and identical boundary conditions are applied. Only the evolution towards this end solution differs. Obviously, it is precisely this evolution that is of interest in the present study.

Prior to auto-ignition, i.e. prior to creation of OH, build-up of the HO_2 radical is clearly visible in Figure 5. HO_2 acts as a precursor to auto-ignition, making it a key intermediate species. This is clearly indicated by the fact that the peak value of HO_2 is reached at a mixture fraction between η_{mr} and η_{st} where OH mass fraction is still very low at that time (Fig. 4). As combustion proceeds, HO_2 is consumed while OH is rapidly generated. The traveling peak of HO_2 from η_{mr} towards the rich side precedes the moving OH peak. These reaction fronts consume the fuel-air mixture. Note that, in contrast to OH, where the peak value rapidly increases by about 2 orders of magnitude compared to the value at $t = \tau_{ign}$, the peak value of HO_2 does not vary strongly in time.

Table 3 reveals that the Konnov mechanism [21] predicts the shortest auto-ignition de-

lay times, while Mueller et al. [16] and Yetter et al. [20] lead to the longest auto-ignition delay times. The most reactive mixture fraction is also at the leaner side for the latter two. The mechanisms of Li et al. [18] and O'Conaire et al. [19] yield nearly identical τ_{ign} values. For the given conditions, auto-ignition first occurs at a mixture fraction between 0.035 and 0.04 (depending on the chemical mechanism, see Table 3), consistent with the findings of [4].

3.1.2 Influence of the co-flow temperature

Figure 6 gives the OH mass fraction evolution for different co-flow temperatures (T_{cf} = 960K, 1003K, 1030K and 1100K) with the Li mechanism [18] and constant scalar dissipation rate ($\langle N \mid \eta \rangle$ = 1s^{-1}). As the co-flow temperature increases, the evolution of OH mass fraction, normalized with τ_{ign}, is slower: the peak moves more gradually towards the stoichiometric mixture fraction. In absolute times, the opposite is true, the higher T_{cf}, the faster the evolution. The "end" results (at $t = 10 \times \tau_{ign}$) are very similar for all values of T_{cf}, with slightly higher OH values for higher T_{cf}.

In [7] it was shown that "time history" of radical concentrations can be used as the indicator of auto-ignition or premixed flame propagation. Auto-ignition is characterized by a build up in the concentration of HO_2 prior to ignition while premixed flame propagation is characterized by simultaneous initiation of build up of all radicals. Figure 7 shows the OH and HO_2 mass fraction evolution for four temperatures at the most reactive mixture fraction. The plots show that, for all temperatures, HO_2 is being generated earlier than OH and is already being consumed as soon as OH is formed. This is consistent with its role as an auto-ignition precursor and indicates that auto-ignition is the stabilizing mechanism, as reported in [3].

As mentioned before, τ_{ign} and η_{mr} depend on the co-flow temperature. Figure 8 shows that, for high enough co-flow temperature ($>$ 1100K), η_{mr} is identical for all mechanisms. With a decrease in co-flow temperature, ignition shifts towards leaner mixture fractions (η_{mr} decreases). This influence of the co-flow temperature is best visible for the lower scalar dissipation rate. In principle, auto-ignition seems to start on the lean side where the local temperature is high enough to allow chemistry to develop. The mechanisms with shorter auto-ignition delay time have richer η_{mr} value, for the entire range of tested co-flow temperatures for low enough scalar dissipation rate. This is not so clear for higher $\langle N \mid \eta \rangle$ values.

The influence of the co-flow temperature on τ_{ign} is shown in Fig. 9 for two different values of N_{max} (with constant scalar dissipation rate). The auto-ignition delay time strongly depends on the co-flow temperature and decreases with an increase in the co-flow temperature. The same trend was observed in the experiments of [4]: the auto-ignition length increases for lower co-flow air temperatures. With increasing co-flow temperature, differences in auto-ignition delay time, as obtained with different mechanisms, diminish. Fig. 9 also reveals that the sharp increase of τ_{ign} occurs only for lower co-flow temperatures for the chemistry mechanisms with the lower τ_{ign}. Finally, note that the different curves do not cross: there are no changes in qualitative behaviour of the mechanisms in terms of the co-flow temperature, as far as τ_{ign} is concerned.

3.1.3 Influence of the conditional scalar dissipation rate

Equations (2) and (3) reveal that the conditional scalar dissipation rate compensates (positive) chemical source terms when $\partial^2 Q_i/\partial\eta^2$ or $\partial^2 Q_T/\partial\eta^2$ is negative. Fig. 4 shows that the second derivative, $\partial^2 Q_i/\partial\eta^2$, is indeed negative around the most reactive mixture fraction at $t = \tau_{ign}$. The higher $\langle N \mid \eta \rangle$, the stronger the term $\langle N \mid \eta \rangle \times \partial^2 Q/\partial\eta^2$ becomes. Thus, it is expected that an increase in N_{max} will increase τ_{ign}. However, from Fig. 3 it becomes clear that, with the AMC model, a substantial increase in N_{max} leads to only a small increase in $\langle N \mid \eta \rangle$ around η_{mr}. Consequently, the impact of N_{max} on the auto-ignition process is small for the current settings when the AMC model is applied. This is

illustrated in Fig. 10 for T_{cf} = 960K and 1030K: the sensitivity of τ_{ign} on N_{max} is small. Obviously, it is more pronounced for lower T_{cf} values (Fig. 10, left), as the chemical source terms become smaller for lower temperatures (and thus the influence of the term $\langle N \mid \eta \rangle \times \partial^2 Q_i / \partial \eta^2$ becomes relatively more important).

For the entire range of scalar dissipation rates, the Konnov [21] mechanism yields the shortest τ_{ign}, while the Yetter mechanism [20] yields the longest τ_{ign}. The mechanisms of Li [18] and O'Conaire [19] yield nearly identical results. The same behaviour is observed for the entire studied temperature range. The different curves again do not cross.

We now consider the sensitivity when $\langle N \mid \eta \rangle = N_{max}$ is applied over the entire mixture fraction range (Fig. 11). The effect on τ_{ign} is much more pronounced now because the region around η_{mr} directly feels the imposed value of the scalar dissipation rate. Still, for high enough T_{cf}, the effect of $\langle N \mid \eta \rangle$ on τ_{ign} is small. As with the AMC model, the curves do not cross and the results are qualitatively similar: the Konnov mechanism [21] yields the shortest auto-ignition delay times over the entire range and Yetter the longest (if it leads to auto-ignition at all). Note that, in all circumstances, the effect of $\langle N \mid \eta \rangle = N_{max}$ on the results with the Konnov mechanism is very small.

3.1.4 Influence of the computational mesh

An accurate prediction of the location of η_{mr} and τ_{ign} requires proper resolution in mixture fraction space. On the other hand, an increase of the number of bins in mixture fraction space increases the computational costs, as all CMC equations have to be solved for each node in composition space as a consequence of the conditioning. For the basic discretization used here, we obtain 10 (9 species plus temperature) x 51 = 510 ordinary differential equations.

In order to examine the influence of the resolution, the mixture fraction space is discretized by means of 21, 51, 101 bins with clustering at the lean side, or with the clustering around stoichiometry, η_{st} (for comparison reasons only). We do this for mechanism of Li et al. [18] and T_{cf} = 1030K, when a constant scalar dissipation rate is imposed over the entire mixture fraction range. Fig. 12 shows the OH mass fraction evolution for the two different clustering choices, with 51 bins. When the bins are clustered around η_{st}, the region around η_{mr} remains clearly under-resolved, even when the relatively high value 51 is used.

A lack of bins at the lean side of the mixture fraction space also leads to an inaccurate prediction of auto-ignition delay times (Fig. 13). Of course this is most clearly visible for the lowest number of bins in mixture fraction space.

Obviously, the value of η_{mr} is not known a priori. Yet, even with the coarse mesh, η_{mr} is quite well approximated (Fig. 12). Therefore, it is relatively easy and fast to construct a computational mesh with sufficient resolution around η_{mr}, starting from a coarse mesh.

3.1.5 Influence of the auto-ignition criterion

As mentioned above, for inhomogeneous mixtures, different auto-ignition criteria can be defined. Here we discuss two criteria. Figure 14 shows the effect of the scalar dissipation rate on the ignition delay time for the criterion of [11] (increase of temperature of 1% over the nominal co-flow temperature). The dependence is identical to what was obtained with the criterion of [10] (Fig. 11). For the present fuel, both criteria thus lead to practically identical results.

3.1.6 Influence of the fuel temperature

Figure 15 shows the influence of the scalar dissipation rate (with the AMC model) on the auto-ignition delay time for cold fuel (T_{fuel} = 305K). The temperature of the co-flow was kept constant (T_{cf} = 1030K). The result for T_{fuel} = 691K is also shown for comparison reasons (Figure 10). Unlike T_{cf}, T_{fuel} has only little effect on the ignition delay time. For T_{fuel} = 305K and N_{max} = 1 s^{-1}, τ_{ign} is 1.43 times longer than with T_{fuel} = 691K, while

a decrease of 140K (from T_{cf} = 1100K to 960K) leads to a 8 times longer τ_{ign}. This is logical: as auto-ignition occurs at η_{mr}, which is very close to zero, variations in T_{cf} are much more directly felt than variations in T_{fuel} (Fig. 1).

3.2 Cabra Flame [5]

3.2.1 Observations during the auto-ignition process

Table 4 shows the auto-ignition delay times, τ_{ign}, for all mechanisms. The differences with Table 3 are striking. For the mechanisms of Mueller et al. [16], Li et al. [18] and Konnov [21], τ_{ign} is an order of magnitude higher than for the Markides case [4]. The Yetter mechanism [20] is even more slower, but the most striking difference is observed for the O'Conaire mechanism [19]. Obviously the most important difference between the Cabra case [5] and Markides case [4] is the fuel (H_2) dilution (Fig. 1). Figures 16 and 17 show the OH and HO_2 mass fraction evolution in time for the Cabra test case [5], normalized with τ_{ign}. Qualitatively, similar observations are found as in Figs. 4 and 5: the HO_2 peak precedes the OH peak in the motion from the lean to the rich side and the first ignition occurs at mixture fractions below 0.1 (Table 4). The maximum OH mass fraction is reached around stoichiometry. It must not be concluded from Fig. 16 and 17 that the evolution with the O'Conaire and Yetter mechanisms is quicker: due to very high τ_{ign} values, the absolute time corresponding to two τ_{ign} is much later.

Interestingly, while the OH levels here are an order of magnitude lower than in Figure 4 (due to the more diluted H_2), the HO_2 levels in Figure 17 are of the same order of magnitude as in Figure 5.

Table 4 reveals that η_{mr} is higher than in Table 3. This is due to the fuel dilution: in addition to a sufficiently high temperature, a sufficient amount of fuel is required to meet the auto-ignition criterion ($Y(OH) = 2 \times 10^{-4}$). Note that also η_{st} is higher than in the Markides case (η_{st} = 0.474 vs. η_{st} = 0.184).

3.2.2 Influence of the co-flow temperature

The influence of the co-flow temperature on η_{mr} and τ_{ign} is shown in Figures 18 and 19 for two values of scalar dissipation rate. As the co-flow temperature decreases, η_{mr} moves towards the richer side, in contrast to the observations in Fig. 8. This is explained below (section 3.3).

The auto-ignition delay time increases with a decrease in co-flow temperature. Figure 19 clearly shows that the Konnov mechanism is the fastest (as in Fig. 9) while the O'Conaire mechanism is now the slowest. Except for the different behaviour of the latter mechanism, the results are qualitatively similar to what was obtained for the Markides case [4] (Fig. 9). Note that, co-flow temperature must be higher here to have ignition, again due to the fuel dilution.

The influence of the co-flow temperature is also seen in the evolution of OH and HO_2 mass fraction for four co-flow temperatures at the most reactive mixture fraction (Figure 20). LES-PDF [12] and RANS-PDF [7, 27] calculations of this test case report that there is no evidence of premixed flame propagation. RANS-CMC simulations [9] on the other hand report stabilization by premixed flame propagation for low temperatures and auto-ignition for high temperatures. Fig. 20 shows that for all temperatures, HO_2 is produced before OH and is already being consumed as OH is formed, as in an auto-ignition stabilized case.

3.2.3 Influence of the conditional scalar dissipation rate

The influence of the scalar dissipation rate is shown in Figure 21, with the AMC model. As the conditional scalar dissipation rate increases, the auto-ignition delay time increases. A critical value of the conditional scalar dissipation, above which auto-ignition does not

occur, is evident for the O'Conaire mechanism. The critical scalar dissipation is lower for lower co-flow temperature. The O'Conaire mechanism is clearly the slowest again, in line with the above. The influence of the scalar dissipation rate is less pronounced when the AMC model is used than when constant scalar dissipation is applied (Fig. 22). The right panels of Fig. 10, 11, 21 and 22, all for T_{cf} = 1030K, clearly show that strong differences are observed due to the differences in fuel dilution. Note that, as it was the case for the Markides configuration, the results with the Konnov mechanism are hardly affected by $\langle N \mid \eta \rangle$.

3.2.4 Influence of the auto-ignition criterion

Figure 23 shows influence of the scalar dissipation rate on τ_{ign} when criterion based on the 1% increase over the nominal co-flow temperature is used. Quantitavely, τ_{ign} is lower than with the OH criterion, but qualitatevely observations are very similar for the Markides [4] and Cabra [5] case.

3.3 Differences and similarities

Common for all mechanisms in both cases is that τ_{ign} increases with decreasing co-flow temperature and increasing conditional scalar dissipation rate (around η_{mr}). The major difference between the two cases is the fuel dilution. There is less fuel (H_2) in the Cabra case than in the Markides case. As a direct consequence, auto-ignition delay times are longer for the Cabra case. Note that the difference in fuel temperature (Table 1) is less important, as η_{mr} is very lean, so that the temperature around η_{mr} (Fig. 1) is comparable for both cases. Whereas this is not surprising per se, it is interesting to note that the sensitivity of the mechanisms is different for both cases, as explained next. The value for τ_{ign} with the O'Conaire mechanism in table 4 is striking, though. Therefore, this is investigated in more detail, in a sensitivity study. For comparison reasons, we also include the Li mechanism in this study. In order to examine the impact of individual reactions on τ_{ign}, the rate of each reaction is changed separately by doubling the pre-exponential factor, repeating the computations for the same conditions (Figs. 24 and 25). The Markides case is less sensitive than the Cabra case. The most important reactions are R1 and R9. Almost identical results are observed for the Markides case for both mechanisms (Fig. 24). For the Cabra case, R1, R2, R3, R4 and R11 speed up auto-ignition while reactions R9, R10, R12 and R13 delay auto-ignition. When the pre-exponential factors of reactions R1, R9, R12 and R13 of O'Conaire mechanism and reaction R9 of Li mechanism are doubled no ignition is observed. The other reactions are less important here. The results are in agreement with findings of [6]. Reaction R9 is the main path to HO_2 production during the pre-ignition phase. The consumption of HO_2 leads to ignition. R11 leads to the production of OH. The difference between Li mechanism and O'Conaire is caused by differences in the reaction rate of reaction R9. Changing only the parameters of reaction R9 in the O'Conaire mechanism to the one from the Li mechanism under the same condition reduces τ_{ign} to 5.335ms, comparable to the Li mechanism results (not shown).

In addition to chemistry sensitivity, a clear qualitative difference between both cases is seen in Fig. 8 and 18: where η_{mr} decreases with decreasing co-flow temperature for the Markides case, it increases with decreasing co-flow temperature for the Cabra case. Figure 26 helps to explain this, from the difference in fuel dilution. The Li mechanism is used here. One must examine the evolution of the mixture fraction position where OH mass fraction is maximum just before auto-ignition (e.g. $t = 0.95\tau_{ign}$) and at auto-ignition time. In the Cabra case (Fig. 26, right), η_{mr} is closer to η_{st} than the mixture fraction where the OH mass fraction is maximal at $t = 0.95\tau_{ign}$. In the Markides case, the opposite is true. The explanation is now as follows: in order to meet the auto-ignition criterion ($Y(OH) = 2 \times 10^{-4}$), there must be sufficient fuel and the temperature must be high enough

to initiate the reaction. In the Markides case, there is always enough fuel, even at very lean circumstances. It only takes longer to meet the criterion Y(OH) = 2×10^{-4} as the co-flow temperature decreases. Consequently, there is more time for the peak value of OH to move to the leaner side (see Fig. 26) and η_{mr} slightly decreases as the co-flow temperature decreases. For the Cabra case, the opposite is true: the mixture fraction where OH mass fraction is maximum, moves to the right in time, looking for fuel to consume. Consequently, as the co-flow temperature decreases, η_{mr} increases as it takes longer to meet the auto-ignition criterion.

4. Conclusions

The auto-ignition processes of heated diluted hydrogen/air mixtures have been numerically simulated by means of an unsteady laminar flamelet approach in mixture fraction space. The sensitivity of the results, obtained with five different chemical mechanisms, to the co-flow and fuel temperature, scalar dissipation rate and fuel dilution, has been investigated. Results were compared for the AMC model and constant scalar dissipation rate over the entire mixture fraction range. The main conclusions are:

- Under all circumstances investigated, the Konnov mechanism given by [21] yields the shortest auto-ignition delay times. The Yetter et al. mechanism [20] yields the longest auto-ignition delay times for the Markides case [4]. For the Cabra case [5], the auto-ignition times are significantly higher and the most striking difference is observed for the O'Conaire mechanism [19].
- A sensitivity study revealed that the settings for the Cabra case [5] make the mechanisms much more sensitive to reaction rates than the Markides case [4]. It also provided the insight to explain the above mentioned difference in behaviour of the O'Conaire mechanism. In particular the reaction for HO_2 formation (R9) is the cause for the strong differences in auto-ignition delay times.
- The differences between different chemical mechanisms are larger for lower co-flow temperatures.
- An increase in co-flow temperature leads to shorter auto-ignition delay times.
- The most reactive mixture fraction corresponds to a lean mixture. It shifts towards the richer side for higher co-flow temperatures for the Markides case [4] and to the leaner side for the Cabra case [5]. This difference in qualitative behaviour is due to the level of fuel dilution.
- With the AMC model, the influence of the maximum scalar dissipation rate, N_{max}, is not strong, because the mixture fractions on the lean side are not strongly affected. When a constant scalar dissipation rate is imposed for the entire mixture fraction range, the influence is much more pronounced.
- Two different auto-ignition criteria give very similar results when the hydrogen is not too strongly diluted [4]. For the Cabra case of [5], the criterion based on temperature [11] gives lower τ_{ign} values than when the OH criterion [10] is used.
- The influence of the fuel temperature is not strong, implying that the differences between two test cases studied are coming mainly from the difference in the fuel composition.
- Clustering of the bins in the mixture fraction space around η_{mr} is necessary to retain accuracy when reducing the computational costs by reducing the number of bins in mixture fraction space.

Acknowledgement

This work has been funded by FWO-project G.0079.07. We thank Prof. Konnov (Lund University) for his fruitful remarks. We acknowledge useful discussions with Prof. E. Mastorakos (Cambridge University) and for providing us CMC code.

References

[1] A.R. Masri, R. Cao, S.B. Pope, G.M. Goldin, *PDF calculations of turbulent lifted flames of H_2/N_2 fuel issuing into a vitiated co-flow*, Combust. Theory Modelling 8 (2004) pp. 1-22.

[2] A.Y. Klimenko, R.W. Bilger, *Conditional moment closure for turbulent combustion*, Prog. Energy Combust. Sci. 25 (1999) pp. 595-687.

[3] I. Stanković, A. Triantafyllidis, E. Mastorakos, C. Lacor, B. Merci, *Simulation of hydrogen auto-ignition in a turbulent co-flow of heated air with LES and CMC approach*, Accepted for publication in Flow Turbul. Combust.

[4] C.N. Markides, E. Mastorakos, *An experimental study of hydrogen autoignition in a turbulent co-flow of heated air*, Proc. Combust. Inst. 30 (2005) pp. 883-891.

[5] R. Cabra, T. Myhrvold, J.Y. Chen, R.W. Dibbel, A.N. Karpetis, R.S. Barlow, *Simultaneous Laser Raman-Rayleigh-Lif measurements and numerical modeling results of a lifted turbulent H_2/N_2 jet flame in a vitiated co-flow*, Proc. Combust. Inst. 29 (2002) pp. 1881-1888.

[6] K. Gkagkas, R.P. Lindstedt, *The impact of reduced chemistry on auto-ignition of H2 in turbulent flows*, Combust. Theory Modelling 13 (2009) pp. 607-643.

[7] R.L. Gordon, A.R. Masri, S.B. Pope, G.M. Goldin, *A numerical study of auto-ignition in turbulent lifted flames issuing into vitiated co-flow*, Combust. Theory Modelling 11 (2007) pp. 351-376.

[8] S.S. Patwardhan, K.N. Lakshmisha, *Auto-ignition of turbulent hydrogen jet in a co-flow of heated air*, Int. J. Hydrogen Energy 33 (2008) pp. 7265-7273.

[9] S.S. Patwardhan, Santanu De, K.N. Lakshmisha, B.N. Raghunandan, *CMC simulations of lifted turbulent jet flame in a vitiated co-flow*, Proc. Combust. Inst. 32 (2009) pp. 1708-1712.

[10] R.R. Cao, S.B. Pope, A.R. Masri, *Turbulent lifted flames in a vitiated co-flow investigated using joint PDF calculations*, Combust. Flame 142 (2005) pp. 438-453.

[11] W.P. Jones, S. Navarro-Martinez, *Study of hydrogen auto-ignition in a turbulent air co-flow using a Large Eddy Simulation approach*, Comput. Fluids 37 (2008) pp. 802-808.

[12] W.P. Jones, S. Navarro-Martinez, *Large eddy simulation of auto-ignition with subgrid probability function method*, Combust. Flame 150 (2007) pp. 170-187.

[13] N. Peters, *Turbulent combustion*, Cambridge University Press, 2000.

[14] H. Pitsch, M. Chen, N. Peters, *Unsteady flamelet modeling of turbulent hydrogen-air diffusion flames*, Proc. Combust. Inst. 27 (1998) pp. 1057–1064.

[15] E. Mastorakos, *Ignition of turbulent non-premixed flames*, Prog. Energy Combust. Sci. 35 (2009) 57-97.

[16] M.A. Mueller, T.J. Kim, R.A. Yetter, F.L. Dryer, *Flow reactor studies and kinetic modeling of the H_2/O_2 reaction*, Inter. J. Chem. Kinet. 31 (1999) pp. 113-125.

[17] C.T. Bowman, R.K. Hanson, D.F. Davidson, Jr Gardiner, V. Lissianski, G.P. Smith, D.M. Golden, M. Goldenberg and M. Frenklach (1999) Gri-Mech 2.11 http://www.me.berkeley.edu/gri mech/

[18] J. Li, Z. Zhao, A.Kazakov, F.L. Dryer, *An Updated Comprehensive Kinetic Model of Hydrogen Combustion*, Inter. J. Chem. Kinet. 36 (2004) pp. 566-575.

[19] M. O'Conaire, H.J. Curran, J.M. Simmie, W.J. Pitz, C.K. Westbrook, *A Comprehensive Modeling Study of Hydrogen Oxidation*, Inter. J. Chem. Kinet. 36 (2004) pp. 603-622.

[20] R.A. Yetter, F.L. Dryer, H.Rabitz, *A comprehensive reaction mechanism for carbon monoxide/hydrogen/oxygen kinetics*, Combust. Sci. Technol. 79 (1991) pp. 97-128.

[21] A. Konnov, *Remaining uncertainties in the kinetic mechanism of hydrogen combustion*, Combust. Flame, 152 (2008) 507-528.

[22] J.V. Michael, J.W. Sutherland, L.B. Harding, A.F. Wagner, *Initiation in H_2/O_2: Rate constants for $H_2 + O_2 - > H + HO_2$ at high temperature*, Proc. Combust. Inst. 28 (2000) pp. 1471-1478.

[23] A. Triantafyllidis, E. Mastorakos, R.L.G.M. Eggels, *Large Eddy Simulations of forced ignition of a non-premixed bluff-body methane flame with Conditional Moment Closure*, Combust. Flame 156 (2009) pp. 2328-2345.

[24] R.J. Kee, F.M. Rupley, J.A. Miller, *Chemkin-II: A Fortran chemical kinetics package for the analysis of gas-phase chemical kinetics*, Sandia, 1989.

[25] E.E. O'Brien, T.L. Jiang, *The conditional dissipation rate of an initially binary scalar in homogeneous turbulence*, Phys. Fluids 3 (1991) pp. 3121-3123.

[26] P.N. Brown, A.C. Hindmarsh, *Reduced storage matrix methods in stiff ODE systems*, J. Comp. Appl. Math. 31 (1989) pp. 40-91.

[27] R. Cabra, J.-Y. Chen, R.W. Dibble, A.N. Karpetis, R.S. Barlow, *Lifted methane-air jet flames in vitiated co-flow*, Combust. Flame 143 (2005) pp. 491-506.

Tables

Table 1. Boundary conditions

Region	Item	Markides [4]	Cabra [5]
Fuel jet	$Y(H_2)$ [-]	0.13	0.0239
	$Y(O_2)$ [-]	0.0	0.00314
	$Y(N_2)$ [-]	0.87	0.972
	$Y(H_2O)$ [-]	0.0	0.00126
	T_{fuel} [K]	691	305
	u_{fuel} [m/s]	120	107
	d [mm]	2.25	4.57
Co-Flow	$Y(H_2)$ [-]	0.0	$0.365\text{x}10^{-4}$
	$Y(O_2)$ [-]	0.233	0.1709
	$Y(N_2)$ [-]	0.767	0.765
	$Y(H_2O)$ [-]	0.0	0.0645
	T_{cf} [K]	945 - 1100	1022 - 1080
	u_{cf} [m/s]	26	3.5
	D [mm]	25	210

Table 2. H_2/O_2 reaction mechanism [16]

R1	$H + O_2 = O + OH$
R2	$O + H_2 = H + OH$
R3	$OH + H_2 = H + H_2O$
R4	$OH + OH = O + H_2O$
R5	$H_2 + M = H + H + M$
R6	$O + O + M = O_2 + M$
R7	$O + H + M = OH + M$
R8	$H + OH + M = H_2O + M$
R9	$H + O_2 + M = HO_2 + M$
R10	$HO_2 + H = H_2 + O_2$
R11	$HO_2 + H = OH + OH$
R12	$HO_2 + O = OH + O_2$
R13	$HO_2 + OH = H_2O + O_2$
R14	$HO_2 + HO_2 = H_2O_2 + O_2$
R15	$H_2O_2 + M = OH + OH + M$
R16	$H_2O_2 + H = H_2O + OH$
R17	$H_2O_2 + H = H_2 + HO_2$
R18	$H_2O_2 + O = OH + HO_2$
R19	$H_2O_2 + OH = H_2O + HO_2$

Table 3. Auto-ignition delay times for Markides test case [4] (Constant scalar dissipation rate, $\langle N \mid \eta \rangle = 1\text{s}^{-1}$, T_{cf} = 1030K, OH based criterion [10]).

Mechanism	τ_{ign} [ms]	η_{mr} [-]
Yetter et al. [20]	0.302	0.0365
Mueller et al. [16]	0.293	0.0365
Li et al. [18]	0.274	0.0409
O'Conaire et al. [19]	0.276	0.0409
Konnov [21]	0.221	0.0409

Table 4. Auto-ignition delay times for Cabra test case [5] (Constant scalar dissipation rate, $\langle N \mid \eta \rangle = 1\text{s}^{-1}$, T_{cf} = 1030K, OH based criterion [11]).

Mechanism	τ_{ign} [ms]	η_{mr} [-]
Yetter et al. [20]	12.19	0.0744
Mueller et al. [16]	6.255	0.0797
Li et al. [18]	4.135	0.0744
O'Conaire et al. [19]	27.34	0.0797
Konnov [21]	1.905	0.0691

Figures

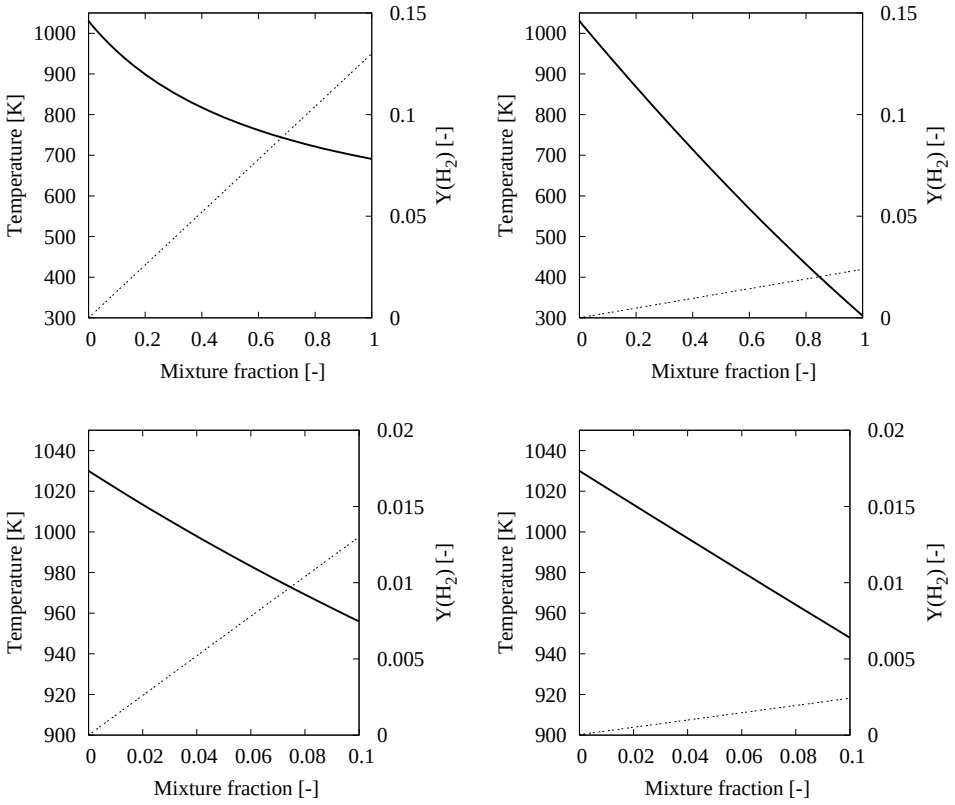

Figure 1. Initial temperature (solid line) and H_2 mass fraction (dashed line) profiles. Left: Markides; Right: Cabra. Bottom: zoom in region: $0< \eta <0.1$ (T_{cf} = 1030K).

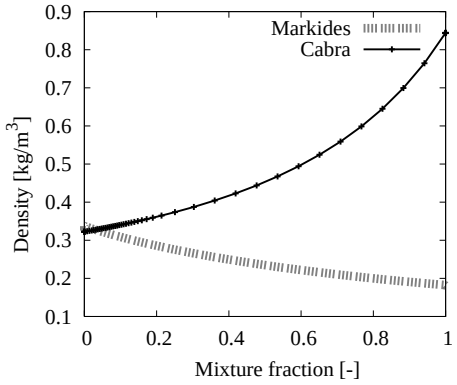

Figure 2. Initial density profiles (T_{cf} = 1030K).

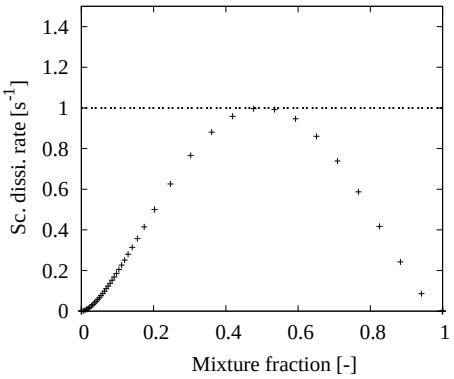

Figure 3. Profiles for conditional scalar dissipation rate: $\langle N \mid \eta \rangle = N_{max}$ everywhere (dashed line), AMC model (crosses) (N_{max} = 1s^{-1}).

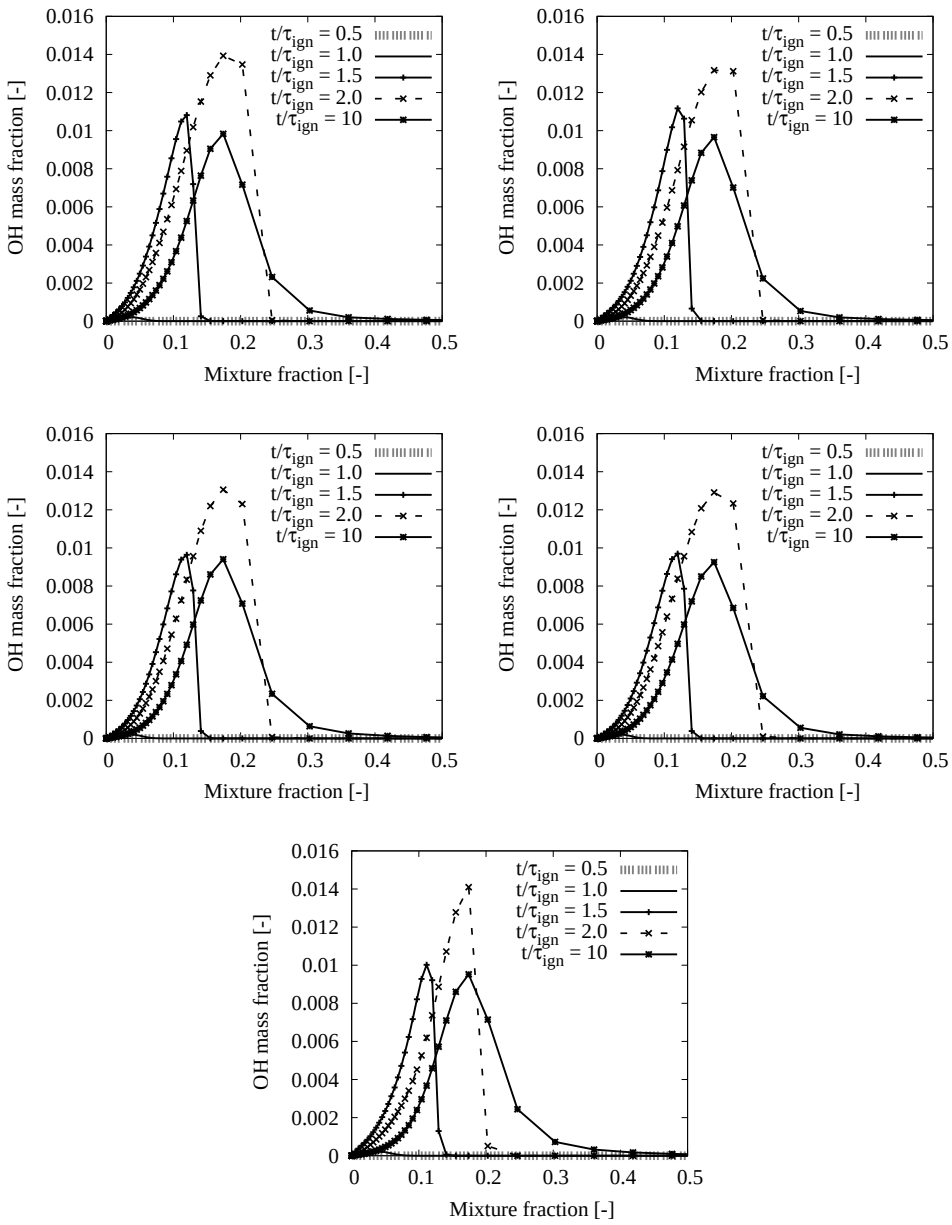

Figure 4. OH mass fraction evolution (T_{cf} = 1030K, $\langle N \mid \eta \rangle = 1s^{-1}$, OH based ignition criterion [10]). Top left: Li et al. Top right: O'Conaire et al. Middle left: Mueller et al. Middle right: Yetter et al. Bottom: Konnov.

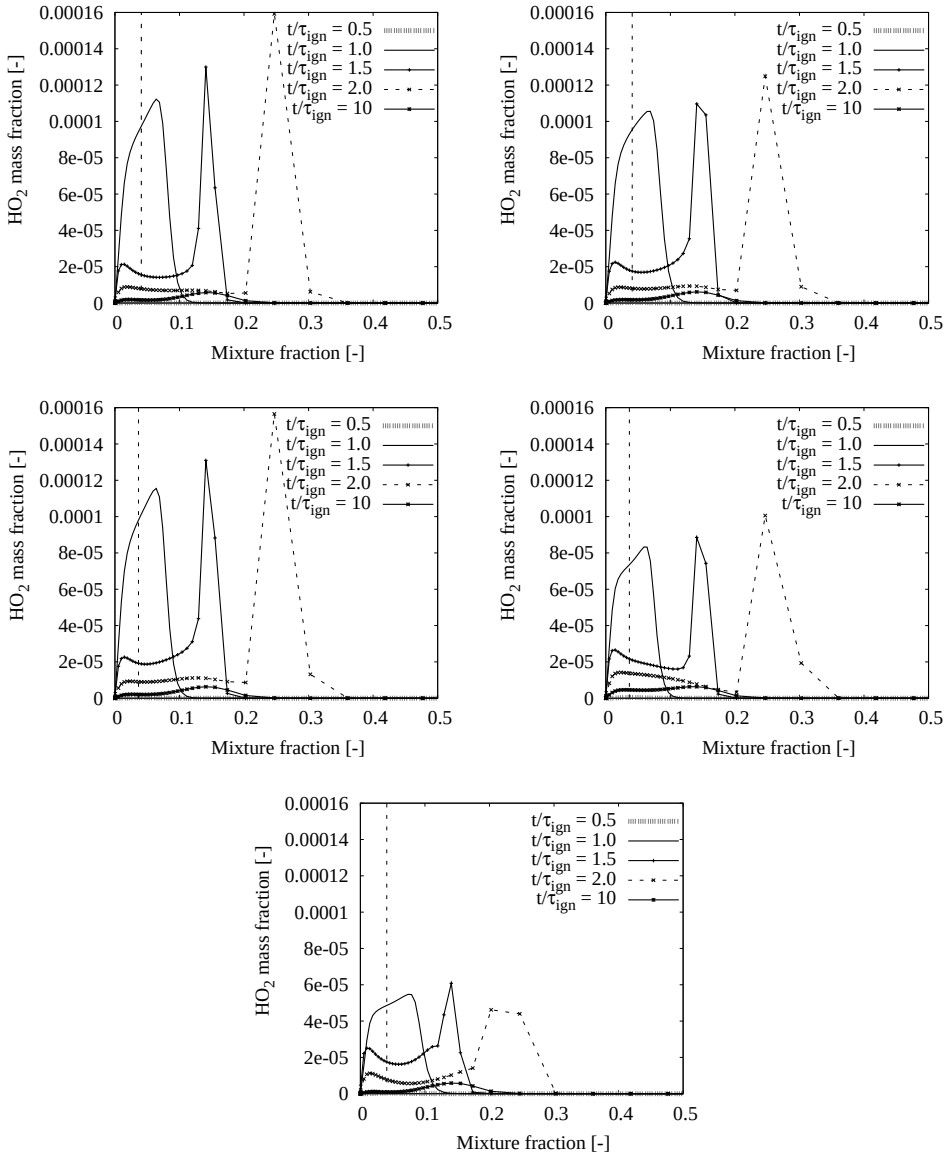

Figure 5. HO_2 mass fraction evolution (T_{cf} = 1030K, $\langle N \mid \eta \rangle = 1s^{-1}$, OH based ignition criterion [10]). Top left: Li et al. Top right: O'Conaire et al. Middle left: Mueller et al. Middle right: Yetter et al. Bottom: Konnov. Vertical dashed line: η_{mr}.

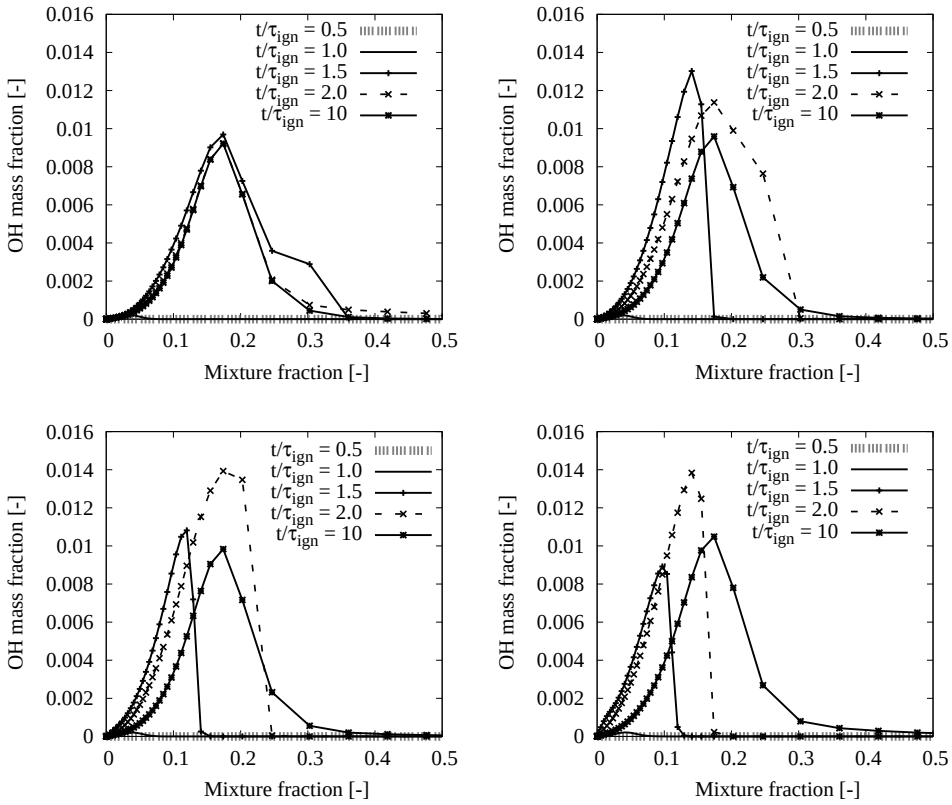

Figure 6. OH mass fraction evolution (Mechanism: Li et al, $\langle N \mid \eta \rangle = 1s^{-1}$, OH based ignition criterion [10]). Top left: T_{cf} = 960K (τ_{ign} = 1.28ms). Top right: T_{cf} = 1003K (τ_{ign} = 0.412ms). Bottom left: T_{cf} = 1030K (τ_{ign} = 0.274ms). Bottom right: T_{cf} = 1100K (τ_{ign} = 0.133ms).

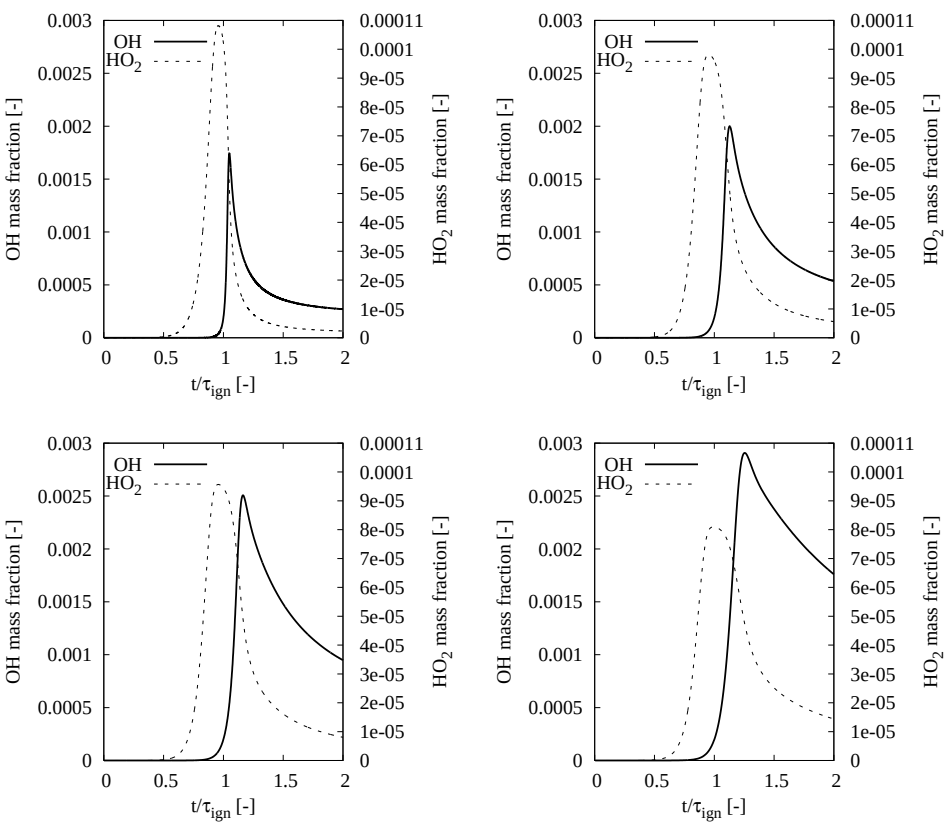

Figure 7. OH and HO_2 mass fraction evolution at η_{mr} (Mechanism: Li et al, $\langle N \mid \eta \rangle = 1s^{-1}$, OH based ignition criterion [10]). Top left: T_{cf} = 960K (τ_{ign} = 1.28ms). Top right: T_{cf} = 1003K (τ_{ign} = 0.412ms). Bottom left: T_{cf} = 1030K (τ_{ign} = 0.274ms). Bottom right: T_{cf} = 1100K (τ_{ign} = 0.133ms).

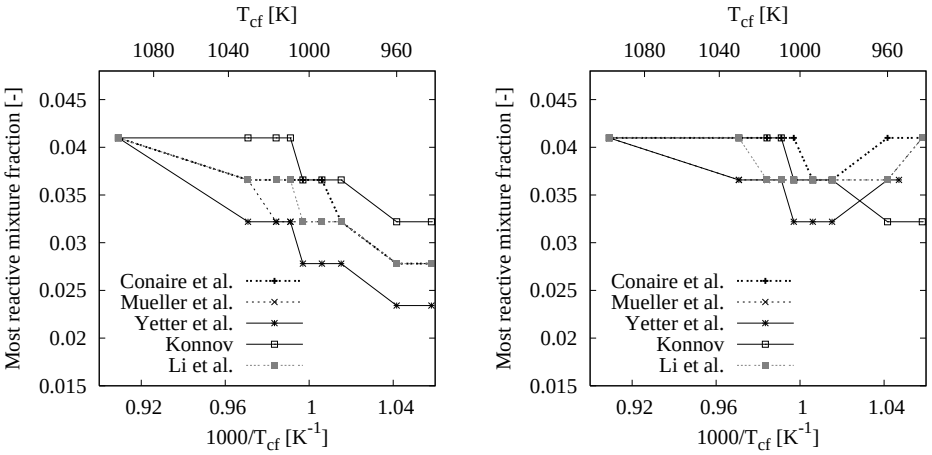

Figure 8. Influence of the co-flow temperature on the location of the most reactive mixture fraction (Constant scalar dissipation rate, left: $\langle N \mid \eta \rangle = 0.1s^{-1}$; right: $\langle N \mid \eta \rangle = 1s^{-1}$).

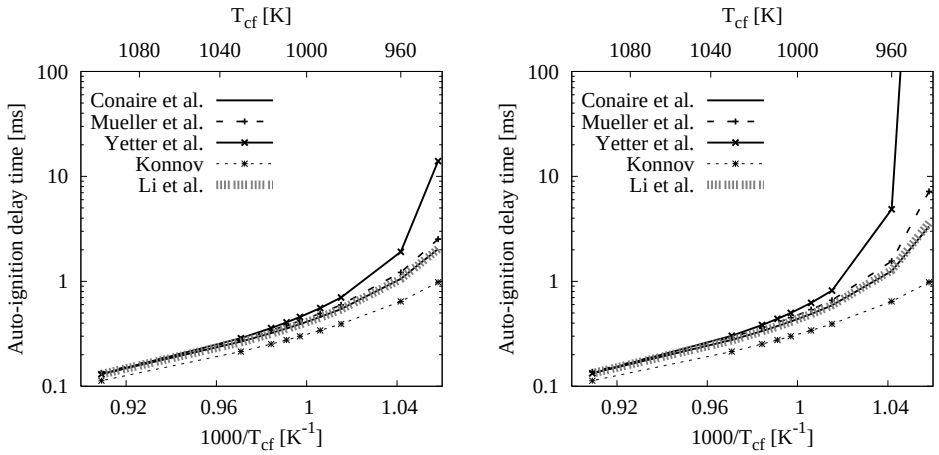

Figure 9. Influence of the co-flow temperature on the auto-ignition delay time. Constant scalar dissipation rate, left: $\langle N \mid \eta \rangle = 0.1\text{s}^{-1}$; right: $\langle N \mid \eta \rangle = 1\text{s}^{-1}$.

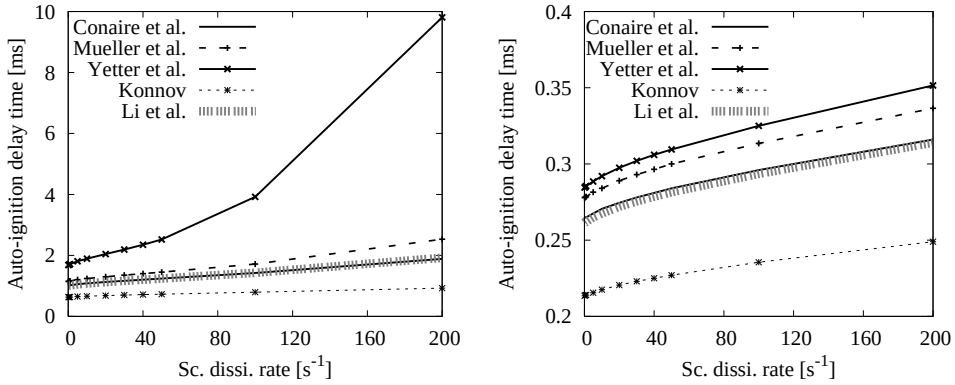

Figure 10. Influence of the scalar dissipation rate on the auto-ignition delay time (AMC model, OH based ignition criterion [10]). Left: T_{cf} = 960K; Right: T_{cf} = 1030K.

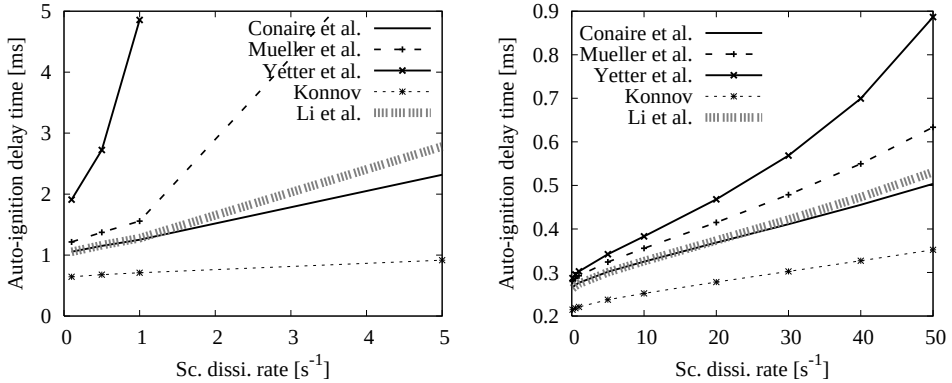

Figure 11. Influence of the scalar dissipation rate on the auto-ignition delay time (constant scalar dissipation rate over entire mixture fraction range; OH based ignition criterion [10]). Left: T_{cf} = 960K; Right: T_{cf} = 1030K.

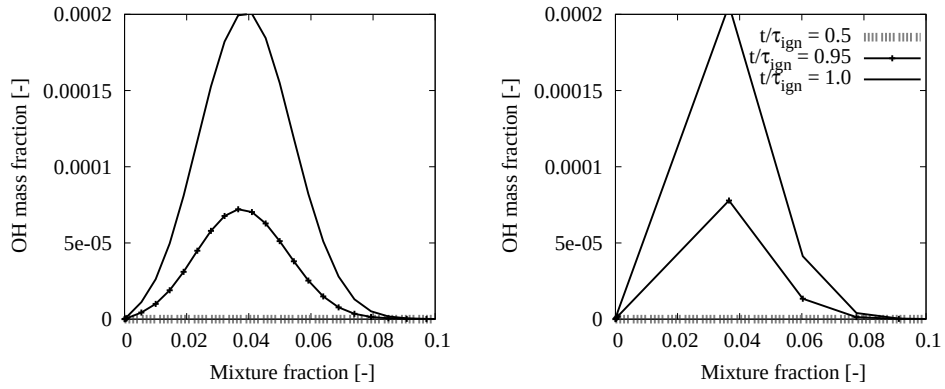

Figure 12. Temporal temperature evolution (T_{cf} = 1030K, $\langle N \mid \eta \rangle$ = 1s^{-1}, 51 bins clustered around mixture fraction 0.04 (left, $\tau_{ign} = 0.274$), and 0.184 (right, $\tau_{ign} = 0.268$)).

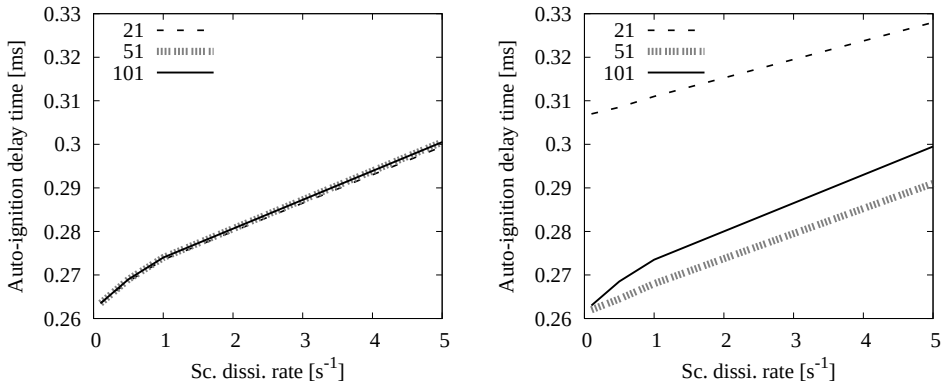

Figure 13. Auto-ignition delay times for different resolutions in mixture fraction space and clustering around mixture fraction 0.04 (left), and 0.184 (right). T_{cf} = 1030K.

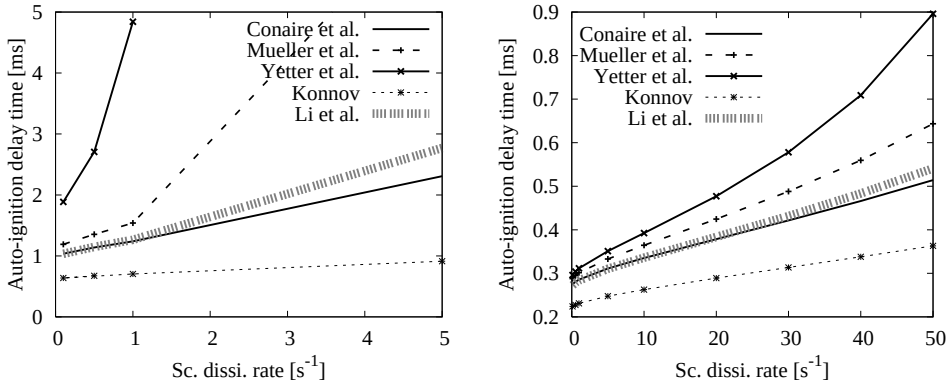

Figure 14. Influence of the scalar dissipation rate on the auto-ignition delay time (constant scalar dissipation rate over entire mixture fraction range; temperature based ignition criterion [11]). Left: T_{cf} = 960K; Right: T_{cf} = 1030K.

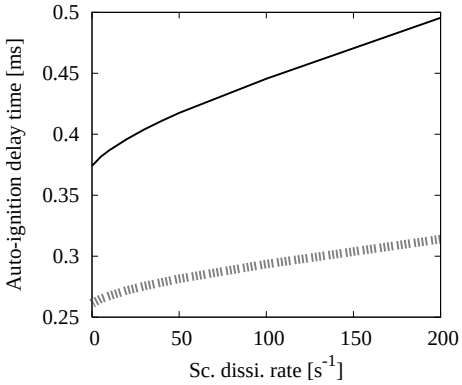

Figure 15. Influence of the scalar dissipation rate on the auto-ignition delay time. Solid line: T_{fuel} = 305K , dashed line: T_{fuel} = 691K (AMC model; Li et al. mechanism; T_{cf} = 1030K ; OH based ignition criterion [10]).

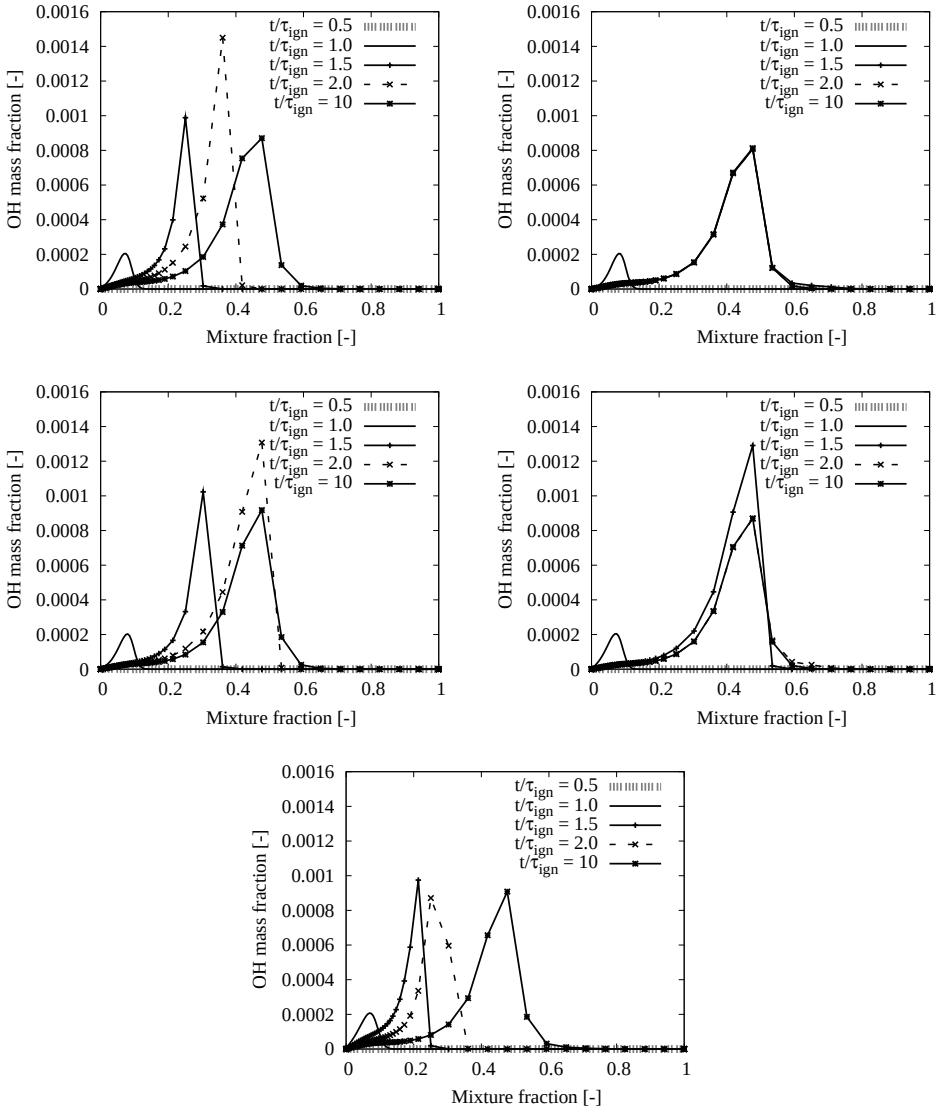

Figure 16. OH mass fraction evolution (T_{cf} = 1030K, constant scalar dissipation rate ($\langle N \mid \eta \rangle = 1s^{-1}$), OH based ignition criterion [10]). Top left: Li et al. Top right: O'Conaire et al. Middle left: Mueller et al. Middle right: Yetter et al. Bottom: Konnov.

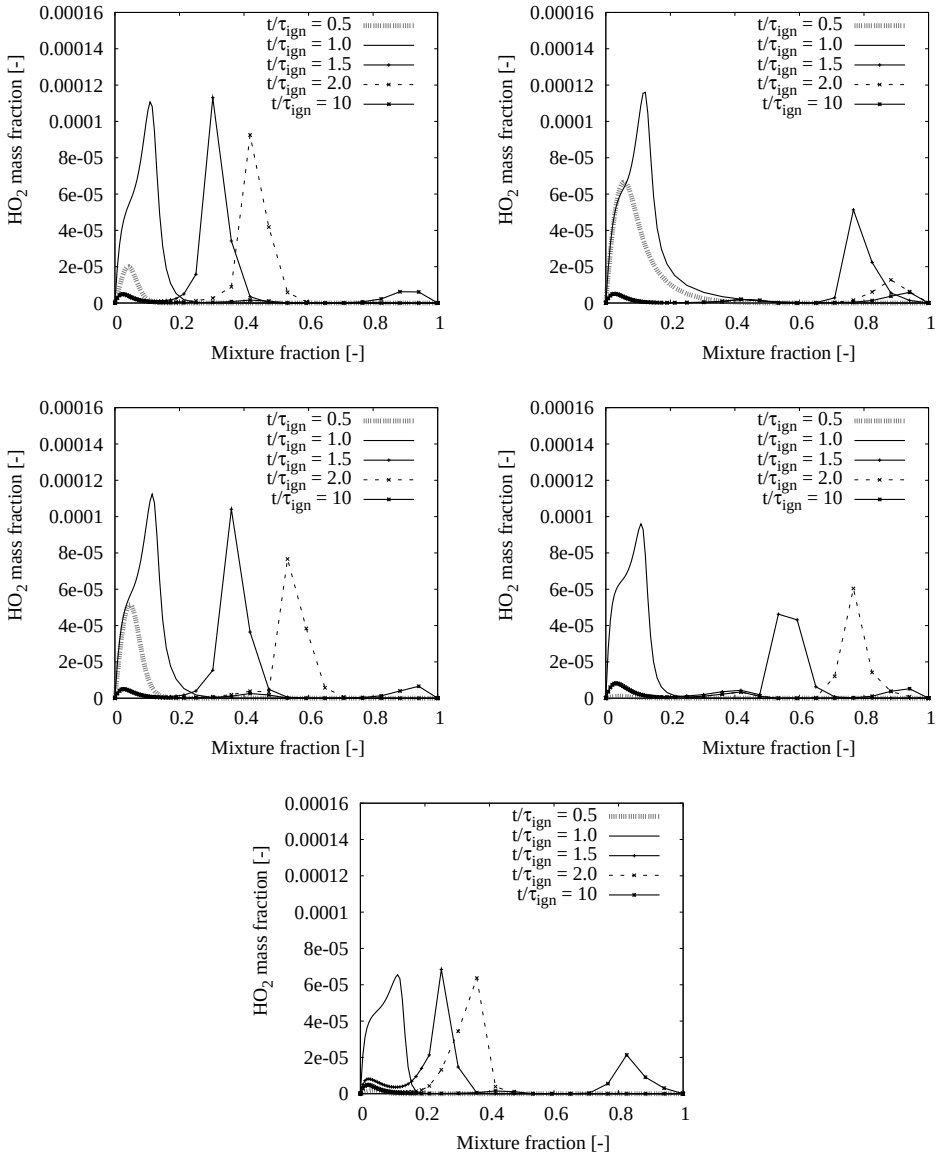

Figure 17. HO_2 mass fraction evolution (T_{cf} = 1030K, constant scalar dissipation rate ($\langle N \mid \eta \rangle = 1s^{-1}$), OH based ignition criterion [10]). Top left: Li et al. Top right: O'Conaire et al. Middle left: Mueller et al. Middle right: Yetter et al. Bottom: Konnov.

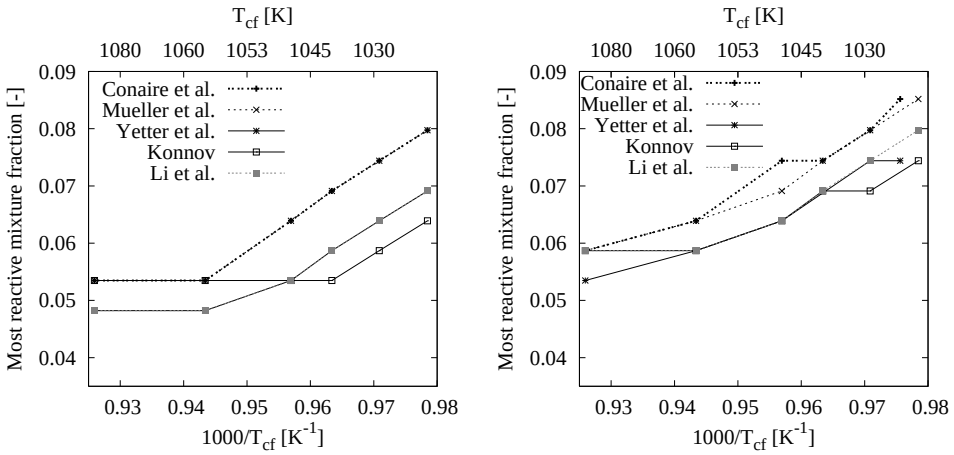

Figure 18. Influence of the co-flow temperature on the location of the most reactive mixture fraction. Constant scalar dissipation rate, left: $\langle N \mid \eta \rangle = 0.1\mathrm{s}^{-1}$; right: $\langle N \mid \eta \rangle = 1\mathrm{s}^{-1}$.

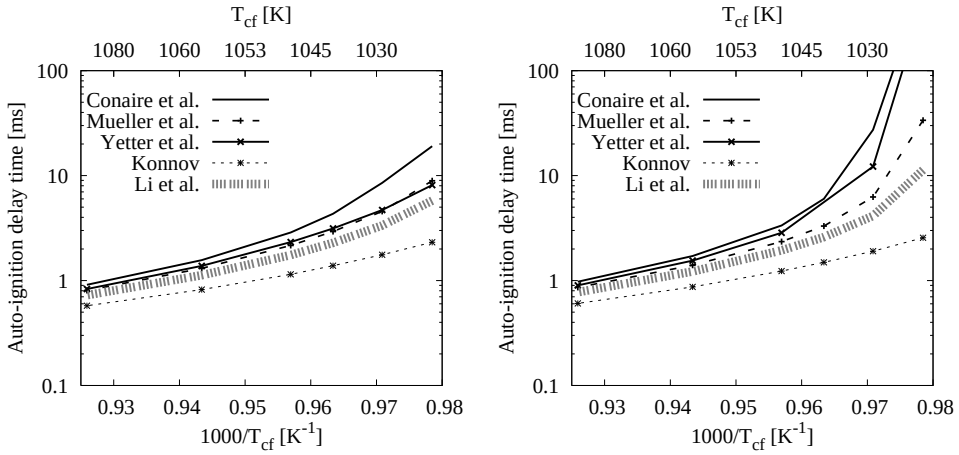

Figure 19. Influence of the co-flow temperature on the auto-ignition delay-time. Constant scalar dissipation rate, left: $\langle N \mid \eta \rangle = 0.1\mathrm{s}^{-1}$; right: $\langle N \mid \eta \rangle = 1\mathrm{s}^{-1}$.

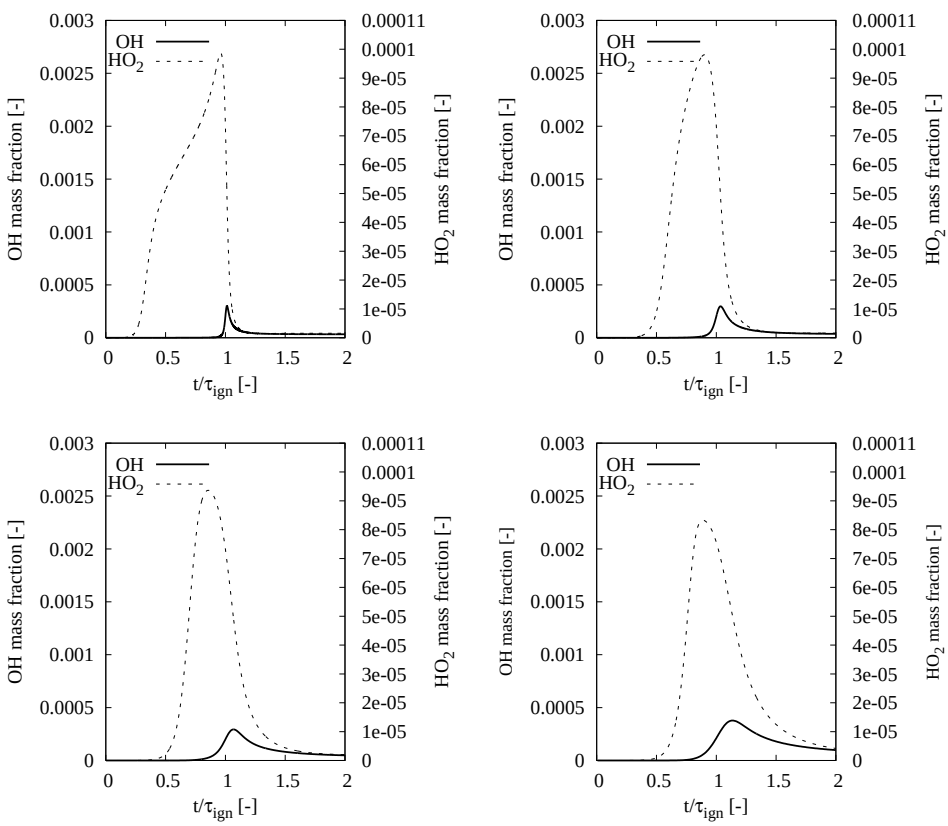

Figure 20. OH and HO_2 mass fraction evolution at η_{mr} (Mechanism: Li et al, $\langle N \mid \eta \rangle = 1s^{-1}$, OH based ignition criterion [10]). Top left: T_{cf} = 1022K (τ_{ign} = 11.33ms). Top right: T_{cf} = 1030K (τ_{ign} = 4.135ms). Bottom left: T_{cf} = 1045K (τ_{ign} = 1.94ms). Bottom right: T_{cf} = 1080K (τ_{ign} = 0.775ms).

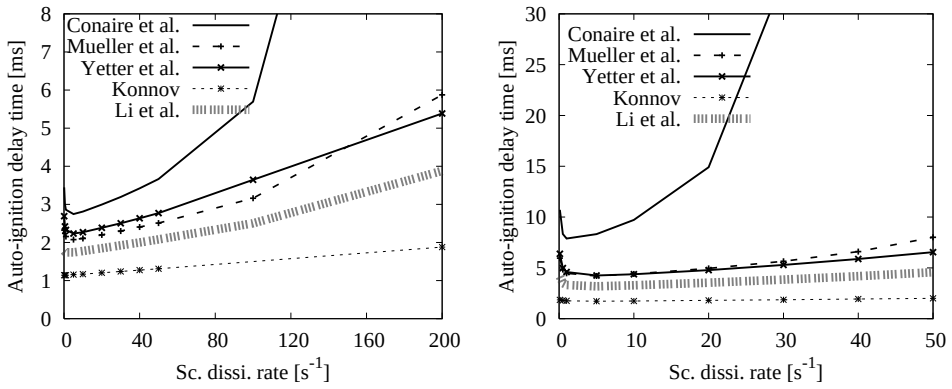

Figure 21. Influence of the scalar dissipation rate on the auto-ignition delay time (AMC model, OH based ignition criterion [10]). Left: T_{cf} = 1045K; Right: T_{cf} = 1030K.

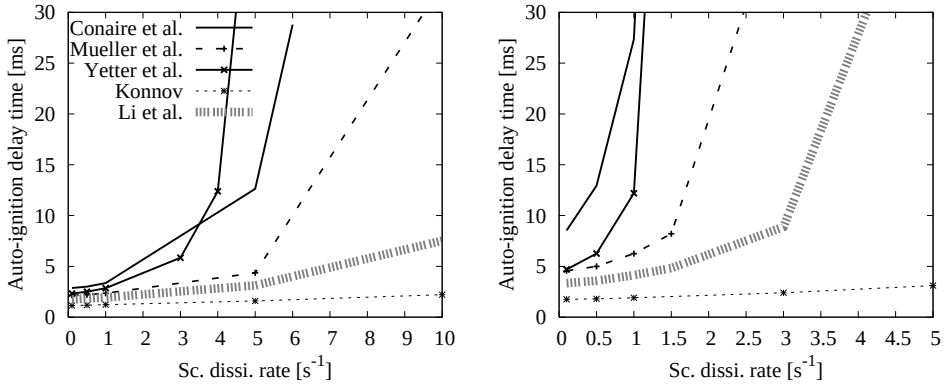

Figure 22. Influence of the scalar dissipation rate on the auto-ignition delay time (constant scalar dissipation rate over entire mixture fraction range; OH based ignition criterion [10]). Left: T_{cf} = 1045K; Right: T_{cf} = 1030K.

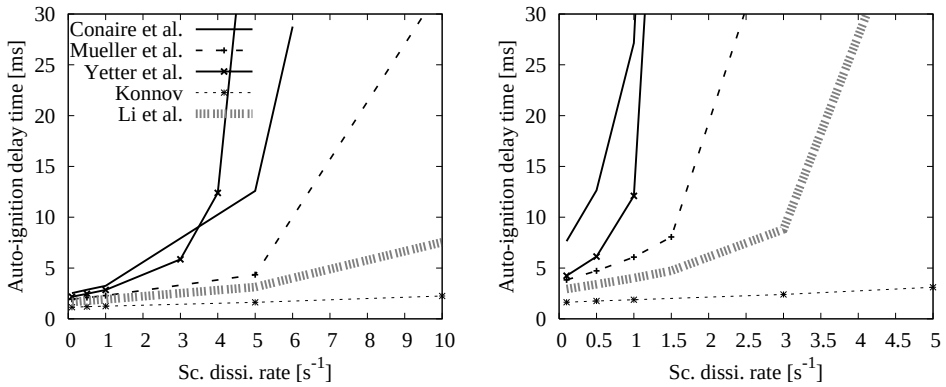

Figure 23. Influence of the scalar dissipation rate on the auto-ignition delay time (constant scalar dissipation rate over entire mixture fraction range; temperature based ignition criterion [11]). Left: T_{cf} = 1045K; Right: T_{cf} = 1030K.

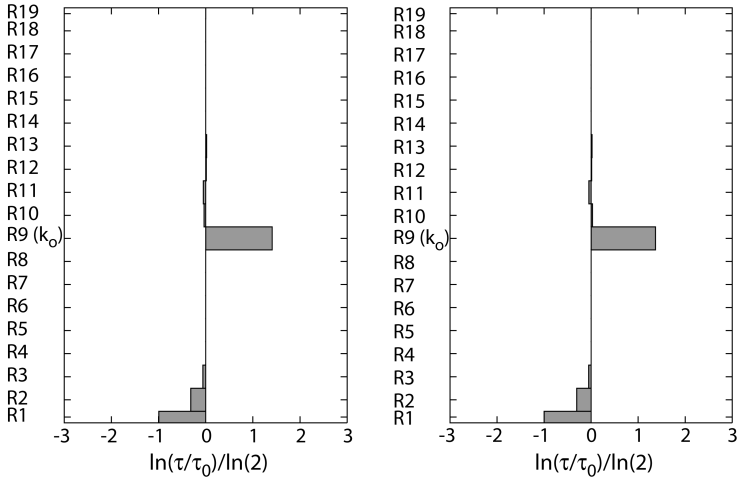

Figure 24. Logarithmic sensitivities of the auto-ignition delay times to changes in reaction rate parameters for the Markides case. Left: Li et al. mechanism; Right: O'Conaire et al. mechanism.

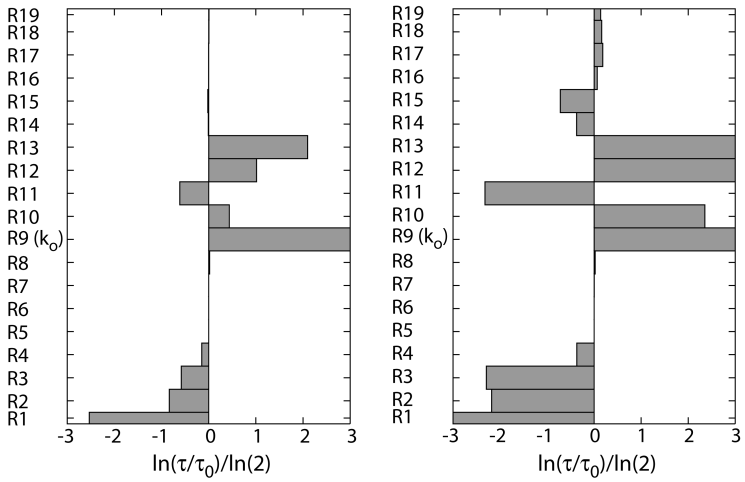

Figure 25. Logarithmic sensitivities of the auto-ignition delay times to changes in reaction rate parameters for the Cabra case. Left: Li et al. mechanism; Right: O'Conaire et al. mechanism.

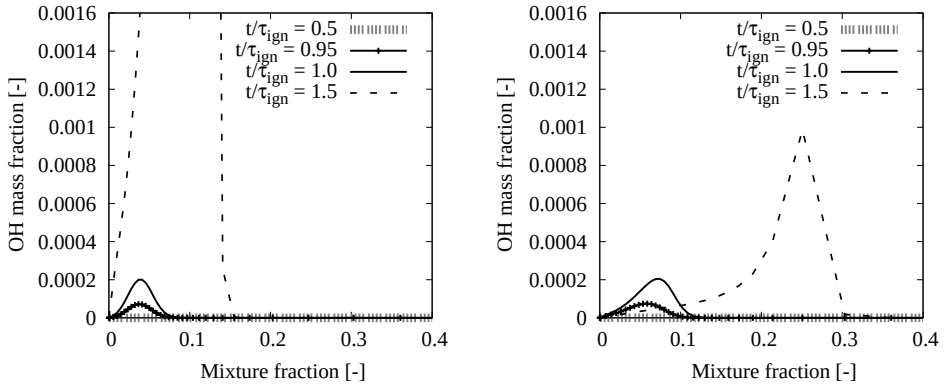

Figure 26. OH mass fraction evolution for Li et al. mechanism (T_{cf} = 1030K; constant scalar dissipation rate: $\langle N \mid \eta \rangle$ = $1s^{-1}$; OH based ignition criterion [10]). Left: Markides test case; Right: Cabra test case.